FULL PAPER

Development and Control of an Articulated Mobile Robot T^2 Snake-4.2 for plant disaster prevention

-Development of M2 arm and C-hand-

Ching Wen Chin[a], Mizuki Nakajima[a], Koki Furuike[a], Kazuyuki Kon[b] and Motoyasu Tanaka[a]

[a] Department of Mechanical Intelligent Systems Engineering, Graduate School of Information Science and Engineering, The University of Electro-Communication, 1-5-1 Chofugaoka, Chofu, Tokyo, Japan;
[b] National Security Solutions Division, NEC Corporation, 1-10 Nisshin-cho, Tokyo, Japan

ARTICLE HISTORY
Compiled October 16, 2022

ABSTRACT
In this study, we develop an articulated mobile robot T^2 Snake-4.2 that can move in narrow spaces, climb stairs, gather information, and operate valves for plant disaster prevention. We develop a novel folding arm M2 arm, fitted to the articulated mobile robot to have a better performance in mobility and operation ability compare to previous work T^2 Snake-4. We introduce a novel method of climbing high steps and stairs by using the M2 arm as a support for the articulated mobile robot. T^2 Snake-4.2 can climb high steps and stairs even with a heavy folding arm. In addition, we present a novel valve operating end effector, C-hand which allows the articulated mobile robot to open a large valve. By utilizing the shape characteristic of the valve, C-hand constraints to the environment and rotates the valve handle without transferring any reaction force to the robot and the folding arm. The developed robot T^2 Snake-4.2 is tested through experiments in the laboratory and also in a field test at the Plant Disaster Prevention Challenge of World Robot Summit 2020.

KEYWORDS
Field Robotics, Articulated Mobile Robot, Folding Arm, Rotating valves, Mobility, World Robot Summit 2020

1. Introduction

Industrial plants that handle hazardous materials such as oil and gas plants are routinely inspected to avoid serious accidents. By sending a remote-controlled robot, humans can inspect hazardous plants safely without risking their lives. Various types of robots have been introduced for plant inspection and disaster response in Autonomous Robot for Gas and Oil Sites(ARGOS) challenge[1] and World Robot Summit(WRS) plant disaster prevention challenge[2]. Quadruped robots such as ANYmal[3] and LIO[4] can maneuver through various terrains by jumping and crawling. Crawler robots such as Quince[5] and FUHGA[6] can move through rough terrain with the crawler mechanisms that cover almost all of the robot body. However, quadruped robots and

CONTACT Ching Wen Chin. Email: chin.ching.wen@rc.mce.uec.ac.jp

crawler robots have difficulties climbing high steps, steep stairs and slopes. During a plant inspection, an accident may happen and an inspection robot is required to move through the rubbles and debris to collect data.

By contrast, articulated mobile robot with high mobility are able to explore complex terrain. Granosik[7] concluded that articulated mobile robots can travel across the rubbles of a collapsed building, squeeze through small crawl spaces to take measurements, perform visual inspections or gather intelligence. Many articulated mobile robots have been developed for disaster response and rescue activities as shown in [8–13].

Matsuno et al. [14] develop Tough Snake Robot Systems to enable robots to carry out plant patrol and inspection. The robots can explore through complex plant structures, such as interior and exterior of pipes, debris, and stairs, and carry out inspections of narrow spaces within buildings. Articulated mobile robot T^2 Snake-3 [15,16] is developed by Tanaka et al. for the application of inspection on roofs, underfloor and industrial plants. T^2 Snake-3 can enter spaces with low headroom, narrow spaces and overcome obstacles. However, it is difficult for the robot to perform heavy-duty operation like lifting an object and opening a valve located high above the ground because the length of the links of the robot are short and the output torque of the joints is limited. ACM-R4 series [17–19] developed by Hirose et al. also can traverse through complex environments but also shared the same weaknesses as T^2 Snake-3.

Installation of a robot arm on an articulated mobile robot is one of the ways to enable it to carry out the inspection and operation tasks high above the ground. Many robot arms for inspection and operation have been developed but most of the arms are more suitable for crawler robots [20–22]. A crawler robot (such as OCTPUS [22]), can handle a long and large arm because it has a large payload. However, an articulated mobile robot is usually lightweight and has low rigidity. The installation of such a long and heavy arm on an articulated mobile robot makes the robot loses some of its mobility to move on rough terrain.

A robot arm is installed on the articulated mobile robot KR-II [23,24] to perform tasks such as grasping and manipulating objects. However, the robot could not pass through spaces with lower headroom because of the height of the robot. Articulated mobile robot T^2 Snake-4 [25] is also developed for plant disaster prevention purpose. A folding arm [26] is fitted on T^2 Snake-4 which enables the robot to access high places and manipulate objects, e.g. rotating valves and opening doors by using an Omni-Gripper [27]. However, the robot could not climb down the stairs because the big size and the heavy weight of the folding arm.

In the present study, we develop an articulated mobile robot T^2 Snake-4.2 for plant inspection purposes. A novel folding arm is developed to enable the robot to access locations high above the ground. A stair climbing method using the folding arm is also proposed to improve the mobility of the robot on ascending and descending steps and stairs. In addition, we also develop a novel end effector, C-hand to rotate the valve that the previous end effector failed to rotate. The effectiveness of T^2 Snake-4.2 has been demonstrated not only through experiments in the laboratory but also in field tests of the Plant Disaster Prevention Challenge in the World Robot Summit 2020 (WRS2020)[28].

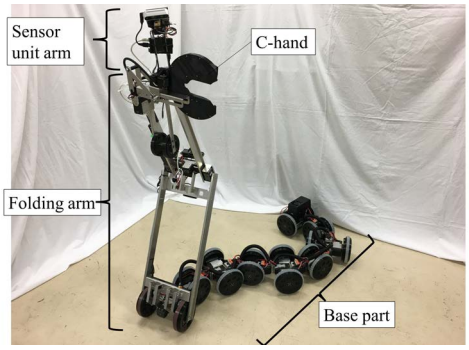

Figure 1. Articulated mobile robot T^2 Snake-4.2.

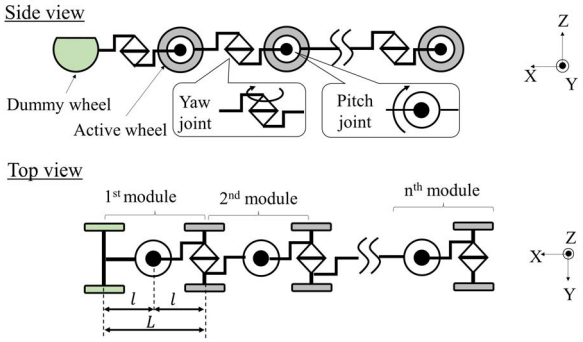

Figure 2. Base part of T^2 Snake-4.2.

Table 1. Parameters of motion area and inspection task in WRS2020

	Value [mm]
Maximum height of step	130
Minimum width of the narrow path	600
Minimum height of low headroom space	1100
Tread and riser of stair	tread: 200, riser: 200
Height of gauges and objects for inspection	500 - 1800
Height of valves	350 - 1800

2. Design of T^2 Snake-4.2

2.1. Design Target

To carry out plant inspection safely, the robot is required to patrol around the plant with various terrains via remote control. The robot also needs to take readings from gauges, detect abnormalities and adjust the operational status of equipment according to the situation. The parameters of the motion area and plant inspection task in WRS2020 Plant Disaster Prevention Challenge[28] are summarized in Table 1. Note that the robot is required to adapt to the changes in the environment and overcome the obstacles when an accident occurs during the inspection. Therefore, the mobility of the robot should not only be limited to the parameters stated in Table 1 such as the overcoming obstacles.

Several tasks have been achieved in the previous articulated mobile robot T^2 Snake-4 [26]. In this study, we focus on the mobility of the robot and the ability to adjust the valves during the inspection. We aim to improve the ability of the robot on ascending

Table 2. Specifications of T^2 Snake-4, T^2 Snake-4.2

	T^2 Snake-4[26]	T^2 Snake-4.2
Number of modules on base part	8	8
Number of joints on folding arm	7	6
Width [mm]	320	280
Height* [mm]	830	750
Maximum height of sensor unit [mm]	1510	1500
Maximum height of end effector [mm]	1100	1270
Mass of base part [kg]	10	10
Mass of folding arm [kg]	7.4	6.5
Mass of end effector [kg]	2.3	0.6
Mass of sensor unit arm [kg]	0.3	0.6
Total mass [kg]	20	17.7

* Height when the folding arm folded in a upright posture

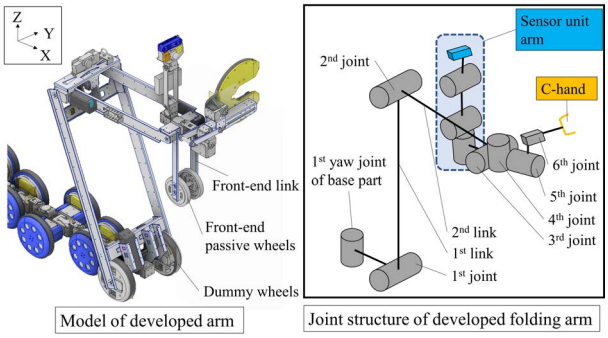

Figure 3. Developed folding arm, M2 arm.

and descending stairs and steps. We also aim to improve the ability of the robot on rotating big industrial valves. Several improvements have been made as stated below on the previous robot and renamed as T^2 Snake-4.2.

(1) A novel folding arm, M2 arm, is developed.
(2) A stair climbing method using the folding arm is proposed
(3) A novel end effector, C-hand, is proposed

Figure 1 shows the developed articulated mobile robot T^2 Snake-4.2. The comparison of the specifications of T^2 Snake-4 and T^2 Snake-4.2 are shown in Table 2. The robot is divided into base parts, folding arm, end effector and sensor unit arm, and the details are described below.

2.2. Base part

The base part of T^2 Snake-4.2 is the same as the previous version, T^2 Snake-4 [25]. The base part is composed of pitch joints and yaw joints serially connected and has active wheels coaxially on the pitch joints, as shown in Figure 2. With the high degrees of freedom, the robot can enter narrow spaces, climb high steps and stairs by controlling its joints and wheels according to the situation. The detailed specification of the base part can be referred to in [25].

Table 3. Specification of joints

Joint	Stall Torque[Nm]	Range(min $\sim$ max)
1^{st} joint (pitch) θ_1	35.1	-60 $\sim$ 125[deg]
2^{nd} joint (pitch) θ_2	35.1	0 $\sim$ 172[deg]
3^{rd} joint (pitch) θ_3	9.6	-110 $\sim$ 120[deg]
4^{th} joint (yaw) θ_4	11.7	-50 $\sim$ 50[deg]
5^{th} joint (roll) θ_5	11.7	-90 $\sim$ 90[deg]
6^{th} joint (prismatic) $\lvert\overrightarrow{WC}_y\rvert$	-	178 $\sim$ 308[mm]

Table 4. Size of parts of the folding arm, M2

Parts of folding arm	Size[mm]
Length of 1^{st} link L_1	650
Length of 2^{nd} link L_2	450
Length of front-end wheel link L_{front}	225
Radius of front-end passive wheel	50
Radius of dummy wheel	75
Width of folding arm	275
x-axis distance of C-hand from wrist $\lvert\overrightarrow{WC}_x\rvert$	64
z-axis distance of C-hand from wrist $\lvert\overrightarrow{WC}_z\rvert$	93

2.3. Folding arm(M2 arm)

With the folding arm, the robot can carry out tasks at locations high above the ground. However, the mobility of the robot was decreased significantly which was caused by the heavy weight of the previous version. Therefore, a novel folding arm, M2 arm, is developed to replace the previous folding arm.

M2 arm is composed of long links serially connected by joints, as shown in Figure 3. The joint configuration of M2 arm is arranged as follows: base part, pitch, pitch, pitch, yaw, roll, prismatic. The configuration is determined as such for the robot to carry out tasks freely in 6 DOF with the end effector and the sensor unit. The orientation of the end effector can be easily determined by the third, fourth and fifth joints as the rotational axes of those joints intersect at one point. The position can be determined by the combination of joints. The specifications of the joints are listed in Table 3. Joints that need to exert a large torque such as the first joint and second joint are fitted with three actuators in parallel. We select the Dynamixel XH540-W270-R and XM430-W350-R (Robotis Co., Ltd.) as the actuators for the joints because they have micro-controllers and the sensors embedded in the units that prevent breakage from overloading and overheating the motors.

The size of each part of M2 arm is set as Table 4 to satisfy the mobility specification in WRS2020 stated in Table 1. The length of the first and second links was originally designed based on the torque limit of the first joint stated in Table 3 so that the folding arm can be elongated horizontally. However, due to the weight of the end effector and the sensor unit arm added to it, the folding arm is unable to elongate as far as expected. The problem could be solved by shortening the length, but it would also reduce the maximum height of the folding arm. Therefore, we maintained the length of each link as designed in Table 4. The link structure of the folding arm is built with lightweight materials such as aluminum alloy 5052 and polylactic acid(PLA) plastic.

M2 arm has a pair of dummy wheels at the first joint and a pair of passive wheels connected to the third joint. The dummy wheels are covered with low coefficient friction materials so that they can be steered freely. The front-end passive wheels are allowed to rotate forward and backward freely but not sideways. This is to prevent

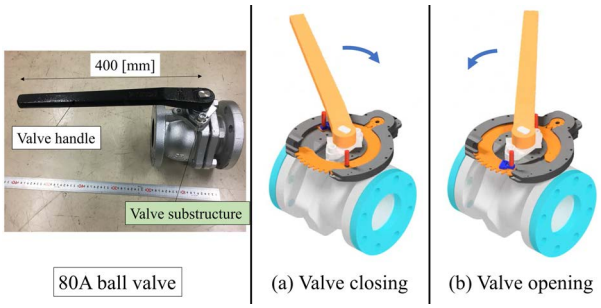

Figure 4. 80A ball valve and its opening and closing direction.

the front-end passive wheels from sliding when the robot climbs stairs or steps. M2 arm is folded when the robot is passing through narrow spaces to avoid obstacles and is unfolded only when carrying out tasks in high places.

2.4. End effector(C-hand)

According to [25], Omni-Gripper [27] that fitted on the T^2 Snake-4 can only rotate valves with a small handle such as 15A ball valve, 50A ball valve and 80A rubber seated gate valve but it is unable to rotate valve with a large handle such as 80A ball valve (Figure 4). To rotate the valves with a large handle, we need to increase the size of the Omni-Gripper. However, the weight of the gripper may be increased accordingly and the mobility of the robot may degrade significantly. The Omni-Gripper could also be replaced with a lighter and simpler end effector such as the parallel gripper proposed in [6,29]. Even with a lighter gripper, the robot is unable to rotate the 80A ball valve because the arm may be twisted by the reaction force from rotating the valve due to the low rigidity of the folding arm.

In this study, we developed a novel end effector, C-hand, as shown in Figure 5, whereby the part of the C-hand constraints to the environment and cancels off the reaction force while opening and closing a valve. It is composed of rotating part, constraint part, and pin posture switching part. C-hand is inserted into the valve's substructure and rotates the handle with the pins fitted on it. By using this method, the length of the valve handle does not affect the ability of the end effector because C-hand does not grasp the valve handle.

C-hand needs to be able to rotate the valve handle 90[deg] clockwise and counter-clockwise to close and open the 80A ball valve. The torque needed to rotate an 80A ball valve was estimated around 30[Nm]. To fulfill the required specifications, the rotating part consists of a motor and a pair of gears and two pins. The position of the pins and the arc of the gears are designed as shown in Figure 5 so that the pins can push the valve handle clockwise and counter-clockwise 90[deg]. We use Dynamixel XH540-W270-R as the motor and a pair of spur gears with a gear ratio of 5.6:1 as the rotating part to ensure C-hand has enough torque to rotate an 80A ball valve.

When the pin pushes the valve handle, the reaction force is shown as red arrows in Figure 6. With the constraint part constraining to the valve's substructure under the handle, the reaction force is compensated. While C-hand opens the valve as shown in Figure 6(b), the reaction force directs the C-hand outwards from the valve's substructure. To ensure the pin is constantly pushing the valve handle while opening the valve, we utilize part of the rotating part to counteract the reaction force. With the constraint part and rotating part, C-hand stays stationary when rotating the valve

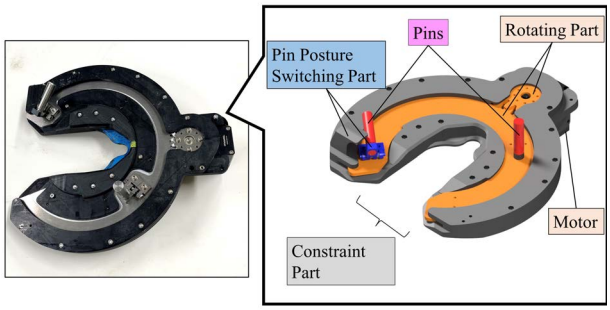

Figure 5. Developed end effector, C-hand.

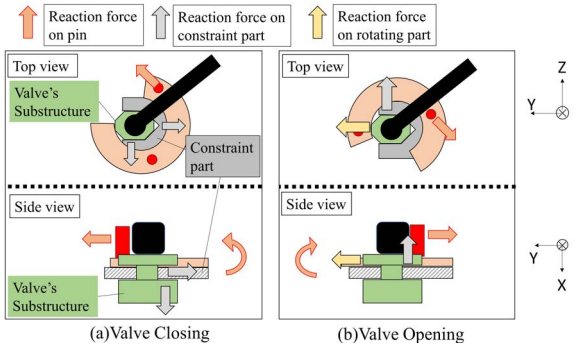

Figure 6. Reaction forces of C-hand when opening and closing a 80A ball valve.(best viewed in color)

handle, therefore, the articulated mobile robot and the robot arm do not sustain any reaction force while opening and closing the valve.

If the pin is fixed vertically, C-hand is unable to be inserted underneath the valve handle as shown in Figure 7(a). A pin posture switching part, composed of a spring-loaded hinge and an L-shaped part, is fitted to the C-hand to push the pin down and the movement is shown in Figure 7(b). By rotating the rotating part counter-clockwise, the pin is pushed down by the L-shaped part so that C-hand can be inserted and withdrawn from the valve's substructure. The pin is raised by the spring after it passes through the L-shaped part. When the rotating part is rotated clockwise, the pin remains standing while sliding sideway around the L-shaped part. The pin is not allowed to be pushed down when rotating in the clockwise direction because it needs to maintain high rigidity to rotate the valve handle.

The design target of rotating big valves could be met by attaching C-hand to the M2 arm as shown in Figure 1.

2.5. Sensor unit arm

To carry out plant inspection task, a sensor unit consists of a visible light camera, a thermal camera, a carbon dioxide sensor and a microphone is used, as Figure 8(a) shows. The sensor unit is fitted on a 3 DOF manipulator (hereinafter: 'sensor unit arm') and the joint configuration is arranged as yaw, pitch, pitch, as shown in Figure 8(b). The sensor unit arm is fitted on the third joint of the folding arm. With this configuration, the sensor unit arm shares the movement with C-hand when first, second and third joint of the folding arm rotates. The sensor unit arm can be controlled

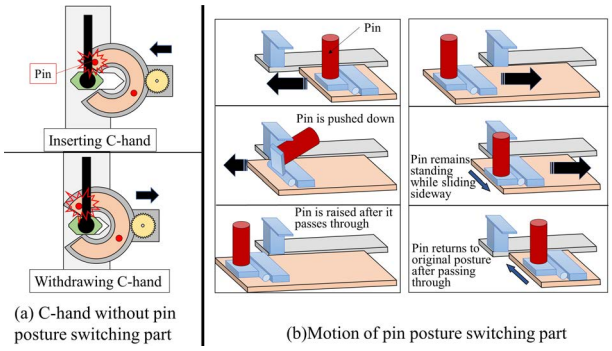

(a) C-hand without pin posture switching part

(b)Motion of pin posture switching part

Figure 7. Pin posture switching part fitted on the C-hand.

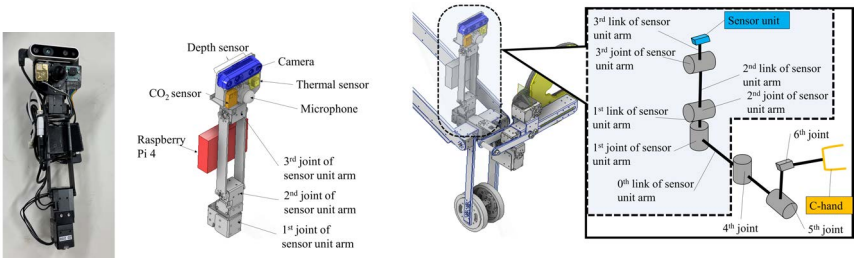

(a) Details of sensor unit.

(b) Joint structure of the sensor unit arm.

Figure 8. Sensor unit arm.

differently based on the control mode.

The sensor unit can be raised to a maximum height of 1500[mm] by extending the folding arm and the sensor unit arm vertically up as shown in Figure 9. We use the Dynamixel XM430-W350-R as the actuators and polylactic acid(PLA) plastic as the link structures.

2.6. Operating system and user interface

Figure 10 shows the operating system of the developed robot. The robot is controlled remotely by an operator from the operator station. In WRS2020, the operating computer is plugged into a wired router that is connected to a Wi-Fi router located in the industrial plant field. The robot can move freely in a narrow environment as it is controlled wirelessly via the Wi-Fi connection. Robot Operating System (ROS) is used as the middleware of the system for communication between computers at the operator station and computers on the robot. The operator uses a gamepad, which is connected to the operating computer, to send commands to the robot. The data accumulated from cameras and sensors are sent back to the computers in the operator station.

Figure 11 shows a screenshot of the operating computer during an inspection. The control mode is shown in the mode area at the bottom of the screen. The posture of the robot is illustrated on the screen to ease the operator in controlling the robot. The numerical information, such as the value of the height of the stair and the calculation time of the control, is indicated in the information area. The error area is used to display any error messages from the actuators such as overload and overheating errors. The camera views are shown on the left side of the screen. The operator operates the robot with all the information provided on the screen.

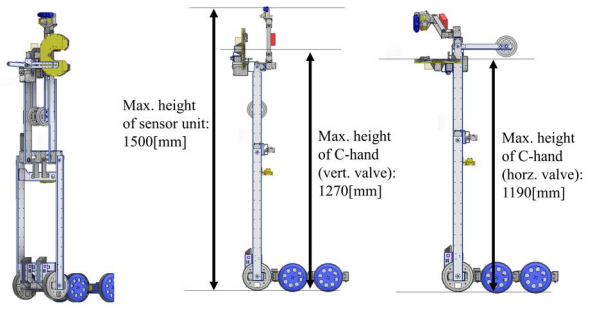

Figure 9. Maximum height of the sensor unit and the C-hand.

3. Controller

Three control modes are implemented in the robot: basic steering control, stairs climbing control, and manipulator control.

3.1. Basic steering control with folding arm

The basic steering control in this paper is similar to the previous version T^2 Snake-4 [25]. The target posture of the robot is determined by a shape-fitting method proposed by Yamada [30]. In the shape-fitting method, the target posture is represented as a continuous curve and the target angles of the joints are approximately calculated by fitting the robot to the curve. The continuous curve is updated by controlling the motion of the head of the robot generated by the operator's commands. This control method is also called shift control because the motion shifts from the head to the tail. In addition, the rotational velocities of the wheels are also calculated based on the continuous curve. The details can be referred to [16,25].

In this section, we discuss about the ideal posture of the folding arm in the basic steering control. Note that the mass of C-hand and the sensor unit arm are concentrated in the front-end of the folding arm. Assuming the weight of C-hand, the sensor unit arm and the other parts at the front-end are acted on third link with a force W_{wrist} as shown in Figure 12(a). Let L_i be the length of i^{th} link, L_{gi} be the distance of the center of gravity of i^{th} link from i^{th} joint, the weight of each element be $\mathbf{w} = [W_1, W_2, W_{wrist}]^T$. The torque act on each joint $\boldsymbol{\tau} = [\tau_1, \tau_2, \tau_3]^T$ can be calculated as follow.

$$\boldsymbol{\tau} = \mathbf{L_g}(\boldsymbol{\theta})\mathbf{w} \tag{1}$$

where

$$\mathbf{L_g}(\boldsymbol{\theta}) = \begin{bmatrix} L_{g1}\sin_1 & L_1\sin_1 + L_{g2}\sin_{12} & L_1\sin_1 + L_2\sin_{12} + L_{g3}\sin_{123} \\ 0 & L_{g2}\sin_{12} & L_2\sin_{12} + L_{g3}\sin_{123} \\ 0 & 0 & L_{g3}\sin_{123} \end{bmatrix}$$

$$\begin{aligned} \sin_1 &= \sin(\theta_1) \\ \sin_{12} &= \sin(\theta_1 + \theta_2) \\ \sin_{123} &= \sin(\theta_1 + \theta_2 + \theta_3) \end{aligned}$$

In contrast, if the front-end passive wheel is grounded, the load on each joint is

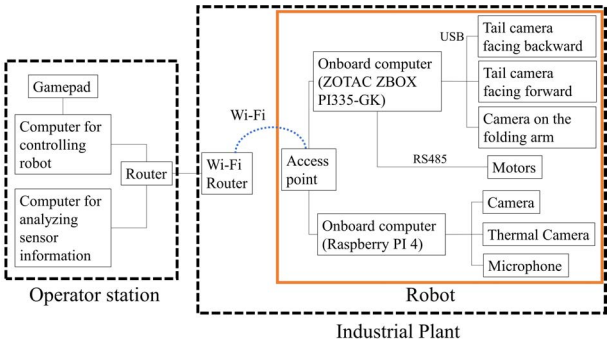

Figure 10. Operating system of the developed robot.

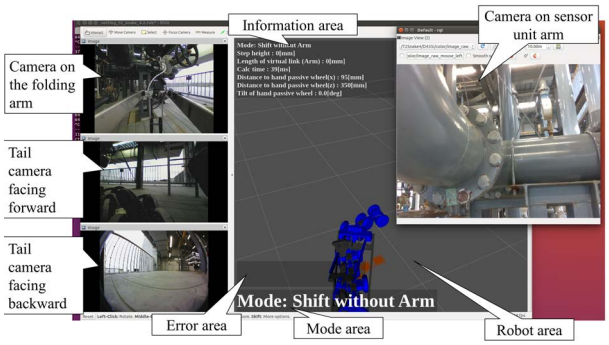

Figure 11. Screenshot of the operating computer during operation.

compensated as shown in Figure 12(b). Let R_3 be the reaction force from the grounded front-end passive wheel. Assuming the front-end passive wheels are located directly under the third joint, the torque act on each joint $\tilde{\boldsymbol{\tau}}$ can be obtained as follow.

$$\tilde{\boldsymbol{\tau}} = \mathbf{L_g}(\boldsymbol{\theta})\mathbf{w} - R_3\mathbf{L_3}(\boldsymbol{\theta}) \tag{2}$$

where

$$\mathbf{L_3}(\boldsymbol{\theta}) = \begin{bmatrix} L_1 \sin_1 + L_2 \sin_{12} \\ L_2 \sin_{12} \\ 0 \end{bmatrix}$$

However, the reaction force of R_3 cannot be solved due to the statically indeterminate problem. There are more unknown variables $(\tau_1, \tau_2, \tau_3, R_1, R_3)$ than the number of equilibrium equations of all the forces and the moments on x-axis and z-axis acting on the structure. We conducted an experiment in Section 4.1 to compare the differences of joint torque in various postures.

In this study, we proposed two handling methods for the folding arm in the basic steering control as shown in Figure 13. Figure 13(a) shows the arm is folded and the front-end passive wheel is rested on the first link. The center of gravity of the folding arm is brought to a position directly above the dummy wheels where the load on the first joint is the least. In this method, the arm is treated as a part of the dummy wheels and the basic steering method is used for only the base part. The operator can steer the head of the base part easily without considering the folding arm in this

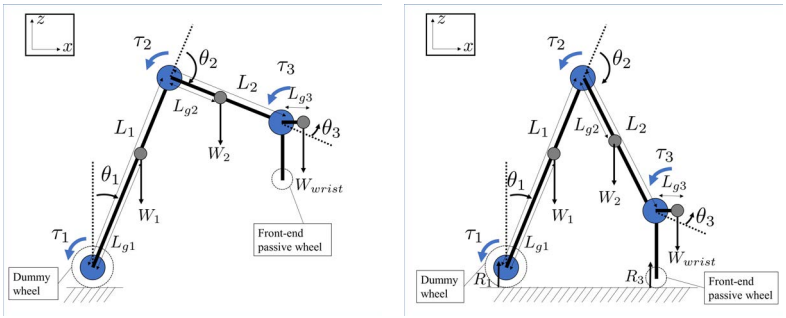

(a) (b)

Figure 12. Simplified model of M2 arm. (a)Posture when front-end passive wheel is lifted. (b)Posture when front-end passive wheel is grounded.

(a) (b)

Figure 13. The handling method of folding arm in the basic steering control. (a) The arm is treated as a part of the dummy wheels. (b) The front-end passive wheels is lowered down.

method. This method is not suitable for climbing obstacles because a large joint torque is needed to lift the entire arm.

Another method is basic steering control while considering the folding arm. The front-end passive wheels are lowered down to touch the ground as shown in Figure 13(b). By contacting the front-end passive wheels to the ground, the joint torque required to lift the head of the robot over an obstacle is reduced as the weight of the folding arm is distributed. The folding arm can also be elongated to contact with a different plane when climbing a higher obstacle. When using this method for basic steering control, the target angles of the joints are calculated using inverse kinematics when the base part is moving. However, the front-end passive wheels are designed not to slip sideways, therefore, the robot is hard to steer sideways.

The height of the folding arm in Figure 13(a) is 700[mm]. The height of the folding arm in Figure 13(b) is 750[mm] but it can be changed by elongating the arm forward when entering spaces with low headroom. The operator can choose the suitable handling method for the folding arm during basic steering control. The operator also can move the sensor unit arm to look around the environment and carry out inspection in this control.

3.2. Stairs climbing control

In [25], a stair climbing method using single backward traveling wave is introduced. The articulated mobile robot can locomote by generating the wave by elongating and

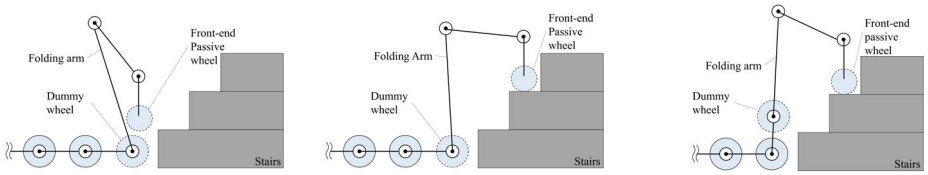

(a) Approaching the stairs. (b) Elongating the arm to a few steps ahead. (c) Performing single backward traveling wave.

Figure 14. Steps of ascending stairs for T^2 Snake-4.2

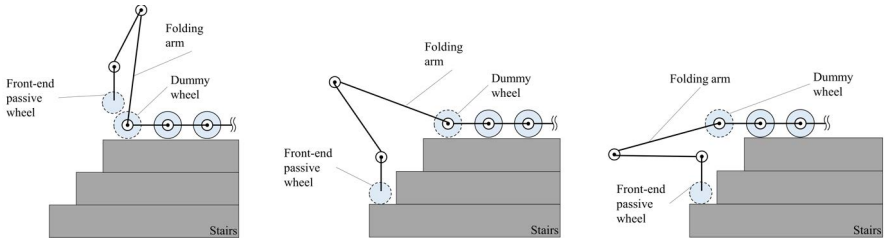

(a) Approaching the stairs. (b) Elongating the arm to a few steps ahead. (c) Performing single backward traveling wave.

Figure 15. Steps of descending stairs for T^2 Snake-4.2.

contracting its body so that it can avoid becoming stuck or falling while climbing stairs. The robot in [25] could climb up the stairs but could not climb down the stairs because the arm is heavy and the link of the arm collided with the tread of the stairs.

In this study, T^2 Snake-4.2 uses a similar method as stated in [25] for stair climbing but with some modifications to the movement of the folding arm. The actuator on the base part is unable to lift the whole folding arm up the stairs due to the heavyweight. We propose a novel stair climbing method by utilizing the high kinematic reachability of M2 arm to support the robot ascending and descending stairs. Figure 14 shows the folding arm is elongated to a few steps ahead manually by the operator before the base part starts ascending the stairs. Next, the base part climbs the stairs by performing the single backward traveling wave, while the front-end passive wheels stay stationary. Note that the joint angles of the folding arm are calculated and controlled based on the movement of the base part to ensure the front-end passive wheels stay grounded. When the dummy wheels reach one step before where the front-end passive wheels are grounded, the front-end passive wheels are lifted and moved to the next plane again. The steps are repeated until the robot finishes climbing the stairs. This method can also be used for the robot descending the stairs, as shown in Figure 15.

The commands of the operator are as follows.

- The position and the orientation of the front-end passive wheel to be elongated to a few steps ahead
- The parameter of the tread and riser of the stairs.
- The forward and backward motion of the base part.
- The timing of shifting each step when performing single backward traveling wave.

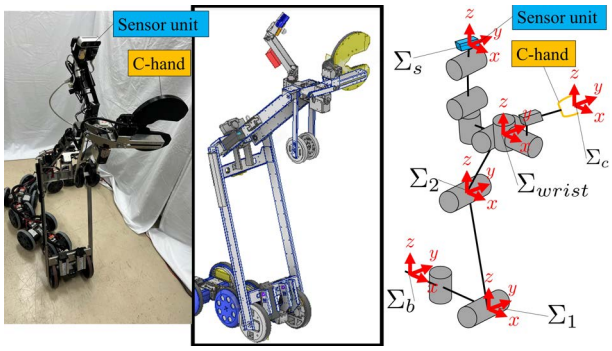

Figure 16. Model of the folding arm for manipulator control.

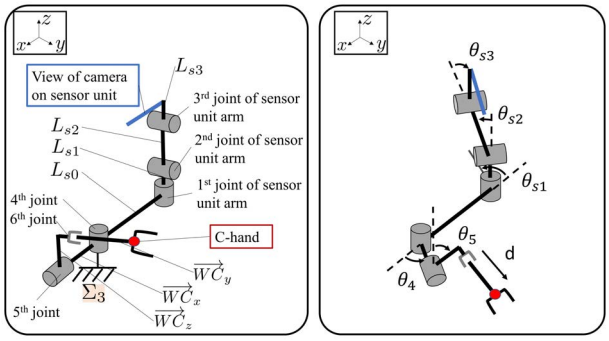

Figure 17. Model of the sensor unit arm and C-hand for manipulator control.

3.3. Manipulator control

3.3.1. Control of the C-hand

In this control mode, C-hand is controlled to be inserted into the valve's substructure as shown in Figure 4. Figure 16 shows the model of the folding arm during the manipulator control. We use not only the joints of the arm but also the first yaw joint of the base part to realize the translational and rotational movement of the end effector. Let Σ_b be the basic coordinate system of the base part, Σ_i be the coordinate system of i^{th} joint, Σ_c be the coordinate system of the center of C-hand, Σ_s be the coordinate system of camera on the sensor unit, and Σ_{wrist} be the wrist coordinate system where the rotational axes of the third, fourth and fifth joints intersect, as shown in Figure 16.

The position and orientation of C-hand, Σ_c is calculated by using the translation transform from Σ_{wrist}. The translation vectors of the x, y, and z axes from Σ_{wrist} to Σ_c are set as $\overrightarrow{WC}_x$, $\overrightarrow{WC}_y$, $\overrightarrow{WC}_z$, respectively. The values of $\overrightarrow{WC}_x$ and $\overrightarrow{WC}_z$ are set constant by the mechanical design as shown in Table 4, while the value of $\overrightarrow{WC}_y$ varies based on the sixth joint controlled by the operator.

There are total seven joints from Σ_b to Σ_c. The sixth joint is controlled separately by the operator to eliminate the kinematic redundancy. Hence, the position and orientation of the C-hand Σ_c from Σ_b is controlled as a 6 DOF manipulator by using inverse kinematics[31,32].

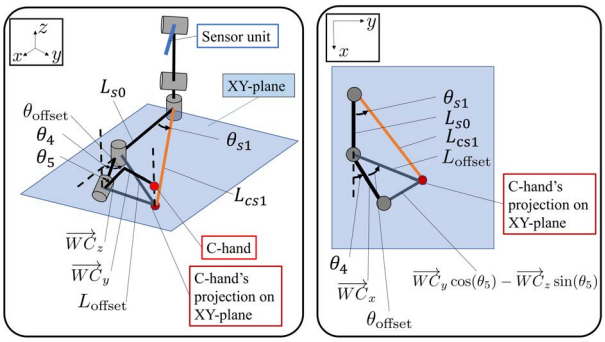

(a) Calculation for θ_{s1}.

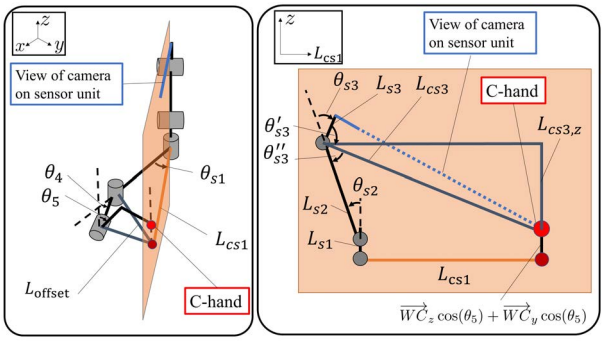

(b) Calculation for θ_{s3}.

Figure 18. Geometric relationships between sensor unit arm and C-hand.

3.3.2. Control of the sensor unit arm

To ensure C-hand always in the view of the visible light camera on the sensor unit arm, the sensor unit arm is controlled relatively to the position of the C-hand. The sensor unit arm is attached to the third link of the folding arm therefore it shares the same coordinate system with C-hand from Σ_b to Σ_3. Figure 17 shows the model of the sensor unit arm and fourth, fifth and sixth joints of the folding arm.

Let θ_i be the angle of the i^{th} joint of the folding arm, and θ_{si} be the angle of the i^{th} joint of the sensor unit arm. Two planes are drawn for easier understanding the relationship between the C-hand and sensor unit arm as illustrated in Figure 18. Let L_{offset} be the distance between the fourth joint and C-hand's projection on plane $x-y$, and θ_{offset} be the angle between fourth link and C-hand. These angles are calculated as below.

$$L_{\text{offset}} = \sqrt{|\overrightarrow{WC}_x|^2 + \left(|\overrightarrow{WC}_y|\cos\theta_5 - |\overrightarrow{WC}_z|\sin\theta_5\right)^2} \tag{3}$$

$$\theta_{\text{offset}} = \text{atan2}\left(|\overrightarrow{WC}_y|\cos\theta_5 - |\overrightarrow{WC}_z|\sin\theta_5,\ |\overrightarrow{WC}_x|\right) \tag{4}$$

Let L_{csi} be the distance between C-hand and i^{th} joint of the sensor unit arm and the value is calculated as follow.

$$L_{cs1} = \sqrt{L_{\text{offset}}^2 + L_{s0}^2 + 2L_{\text{offset}}L_{s0}\cos(\theta_{\text{offset}} + \theta_4)} \tag{5}$$

$$L_{cs3,z} = L_{s2}\cos\theta_{c2} + L_{s1} - |\overrightarrow{WC}_z|\cos\theta_5 - |\overrightarrow{WC}_y|\sin\theta_5 \tag{6}$$

$$L_{cs3} = \sqrt{L_{cs3,z}^2 + \Big(L_{cs1} - L_{s2}\sin\theta_{s2}\Big)^2} \tag{7}$$

The second joint of sensor unit arm is controlled separately by the operator to eliminate the kinematic redundancy. By rotating the second joint of the sensor unit arm θ_{s2}, the sensor unit can be moved nearer or further to the C-hand on plane L_{cs1}-z, as shown in Figure 18(b). The joint angles θ_{s1} and θ_{s3} of the sensor unit arm are calculated as below

$$\theta_{s1} = \text{atan2}\Big(L_{\text{offset}}\sin(\theta_4 + \theta_{\text{offset}}),\ L_{c0} + L_{\text{offset}}\cos(\theta_4 + \theta_{\text{offset}})\Big) \tag{8}$$

$$\theta_{s3} = \pi - \theta'_{s3} - \theta''_{s3} \tag{9}$$

where

$$\theta'_{s3} = -\text{atan2}\Big(L_{cs3,z},\ L_{cs1} - L_{s2}\sin\theta_{s2}\Big) - \theta_{s2} + \frac{\pi}{2} \tag{10}$$

$$\theta''_{s3} = \text{acos}\left(\frac{L_{s3}}{L_{cs3}}\right) \tag{11}$$

4. Experiments

Experiments were carried out to verify the effectiveness of the developed robot T^2 Snake-4.2 and the control modes proposed in previous section.

4.1. Comparison of the posture of the folding arm

We carried out experiments for six cases to compare the load on each joint based on the posture of the folding arm as shown in Figure 19. In cases (a) and (b), the joint angles were set as such that the center of gravity of the folding arm was located above the dummy wheel. The front-end passive wheels were lifted in case (a) while they were rested on the first link of the folding arm in case (b). In cases (c) and (d), the folding arm was folded in an upright posture. The front-end passive wheels were lifted slightly from the ground in case (c) while they were rested on the floor in case (d). In case (e), the folding arm was elongated horizontally by the second joint. In case (f), the folding arm was elongated in an upright posture. In a DC motor, the output torque is directly proportional to the current input. Therefore, the current I[A]of each joint was measured every 0.1[s] by maintaining the target angle for 10[s] for each case. The average was taken to compare the torque output of each joint.

Figure 20 shows the differences in the value of current based on every case. In cases (a) and (b), the current of the first joint was similar because the center of gravity of both cases was nearly the same. In case (b), the load on the second joint was compensated by resting the front-end passive wheel on the first link. The current of

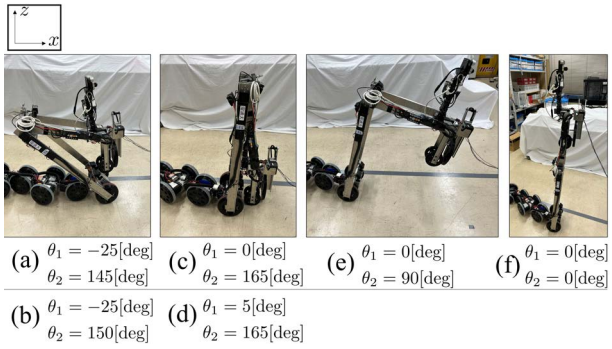

Figure 19. Comparison of six cases of posture for folding arm.

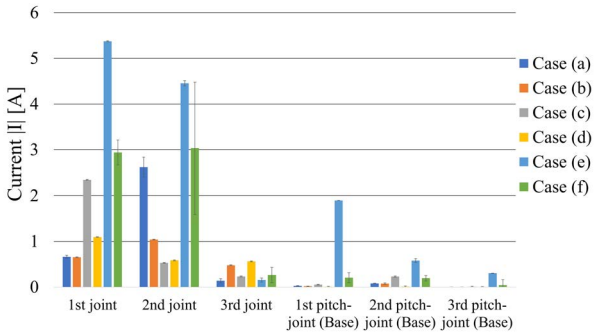

Figure 20. Experimental results of six cases of posture for folding arm.

Figure 21. Problem occured when the folding arm extended forward.

the first joint in case (c) was large because the center of gravity was located in front of the dummy wheel. However, when the front-end passive wheel is rested on the ground in case (d), the load was compensated.

In case (e), the current of the first and second joints were the largest because the distance of the center of gravity from the dummy wheel was the farthest among the cases. Figure 21 shows the base part was lifted when the folding arm was extended forward. The pitch joints of the first few modules on the base part exerted a high amount of torque to balance the posture of the folding arm. The reason for that is the moment created by the weight of the folding arm was greater than the weight of the first few modules of the base part. The wheels of these modules are ungrounded and cannot generate propulsion force as expected for mobility.

Therefore, the folding arm is recommended to stay folded in basic steering mode. The experiment shows the loads on the joints were reduced by resting the front-end passive wheels on the ground or an object.

Table 5. Comparison of the mobility of T^2 Snake-4 and T^2 Snake-4.2

Mobility	T^2 Snake-4	T^2 Snake-4.2
Minimum width of the L-shaped corridor	400mm	400mm
Maximum step height without riser	400mm	800mm
Maximum step height with riser	600mm	800mm
Ability of climbing up stairs (tread: 200mm, riser: 200mm)	Success	Success
Ability of climbing down stairs (tread: 200mm, riser: 200mm)	Failure	Success

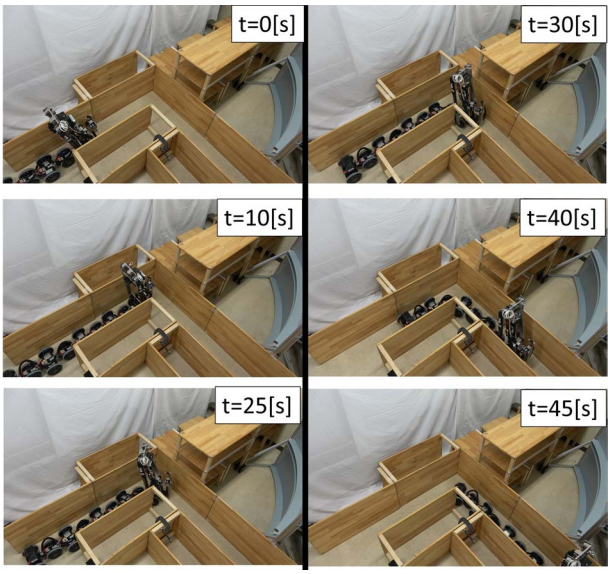

Figure 22. Experiment of passing through an L-shaped corridor. (width=400mm)

4.2. Mobility of T^2 Snake-4

Table 5 shows that the mobility of T^2 Snake-4.2 has significantly improved compared to the previous version T^2 Snake-4. In these experiments, the robot was controlled by the operator using a gamepad while directly looking at the robot.

Figure 22 shows that the robot could steer through an L-shaped corridor with a width of 400[mm]. The robot fulfilled the ability to traverse through a narrow path stated in Table 1. The robot was controlled in the basic steering control mode. Note that the folding arm was folded in the posture shown in case (c) as shown in Figure 20. The front-end dummy wheel was lifted from the floor slightly so that the robot could steer freely.

Figure 23 shows the robot could climb a higher step with the height of 800[mm] thanks to the novel folding arm. The folding arm could reach the plane of a higher step because it has longer links and lighter weight on the folding arm than the previous version. By elongating the folding arm to the next plane ahead, the weight of the folding arm was distributed and the robot was able to climb up or down the step easily without falling. The maximum height was limited to the reachable height of the front-end passive wheels.

Stair climbing experiments were carried out using the method proposed in Section 3.2. Figure 24 shows the robot could ascend and descend the stairs with tread width of 200[mm] and riser height of 200[mm]. The target position of the front end passive wheels relative to the dummy wheels when ascending and descending stairs is shown in the Figure 25. The folding arm was elongated to two steps ahead before the base part

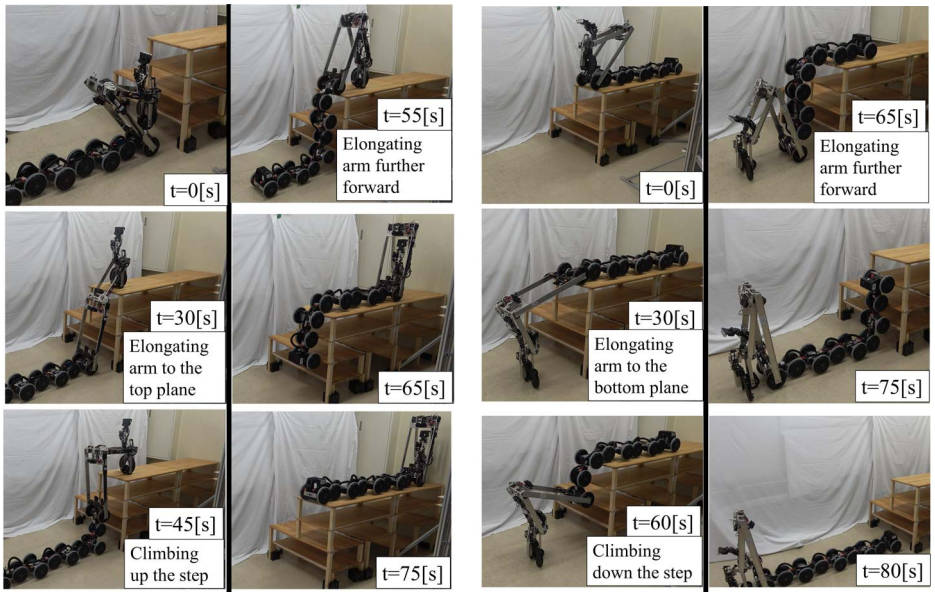

(a) Climbing up step.(800mm) (b) Climbing down step.(800mm)

Figure 23. Experiment of step climbing.

Table 6. Time consumed for ascending and descending stairs

	Ascending stairs	Descending stairs
Elongating arm to next step	74[s] (30.5%)	97[s] (32.3%)
Elongating arm forward	30[s] (12.3%)	29[s] (9.7%)
Performing single backward traveling wave and moving forward	139[s] (57.2%)	174[s] (58.0%)
Total time consumed	243[s]	300[s]

started ascending the stairs. After the base part climbed the first step of the stairs, the folding arm was elongated further to two steps ahead before the base part continued climbing. The folding arm could not be elongated more than two steps ahead due to the torque limit of the joints of the folding arm.

In contrast, the robot does not need to lift up the folding arm when descending the stairs. The folding arm could be elongated to the bottom of the stairs and remained contact with the tread of the stairs by rolling the front-end passive wheels forward step by step without overloading the joints. Therefore, the folding arm was elongated less frequent when descending stairs than ascending stairs.

The time consumed for ascending and descending the stairs is shown in Table 6. The result shows that the time consumed for performing single backward traveling wave and moving forward is the longest. It is because the operator needs to be careful that the wheel does not get stuck under the open riser stair. Introduction of automation control for stair climbing to shorten the time consumed is a task for future work.

4.3. Ability of C-hand on valves rotating

Figure 26 shows the proposed end effector, C-hand opening and closing the 80A ball valve. C-hand was able to rotate the handle of the valve without any support. By constraining to the valve's substructure, the reaction force was compensated and C-hand stayed stationary.

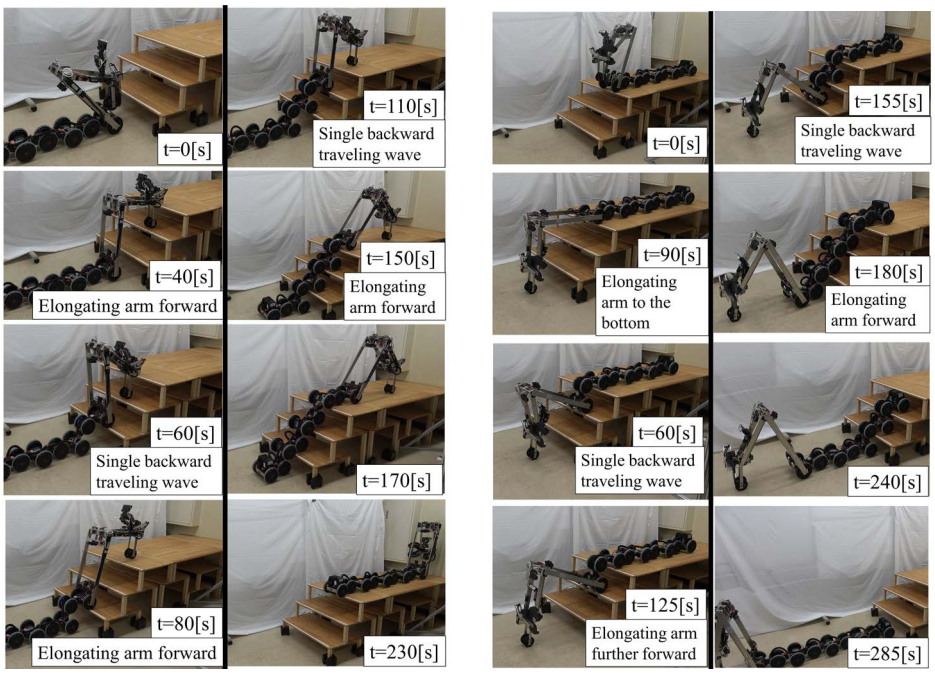

(a) Ascending stairs. (b) Descending stairs.

Figure 24. Experiment of stairs climbing.

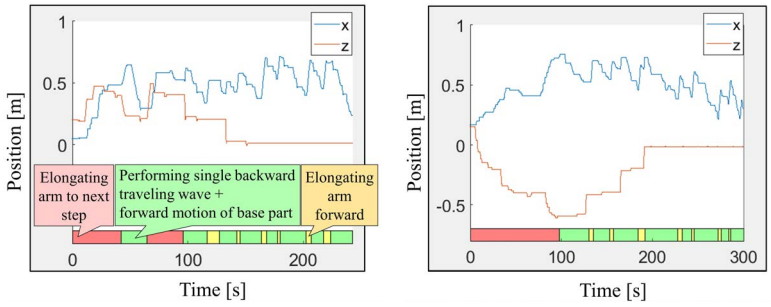

(a) Ascending stairs. (b) Descending stairs.

Figure 25. Target position of front-end passive wheels relative to dummy wheels during stairs climbing.

By fitting C-hand on the folding arm, the robot was able to rotate valves located in various position and orientation. Figure 27 shows the robot rotate the valves with the orientations as they are fitted on a vertical pipe or a horizontal pipe. As the result, the articulated mobile robot and the robot arm did not sustain any reaction force when C-hand was opening and closing the valve. Note that the position of the valve needs to be in front or on the left side of the robot because C-hand is fitted facing the left side of the folding arm.

4.4. Ability of sensor unit arm

Figure 28 shows that the sensor unit could be raised to a maximum height around 1500[mm] and collect data from different directions thanks to the degree of freedom of the sensor unit arm.

Experiment on the movement of sensor unit arm during the manipulator mode

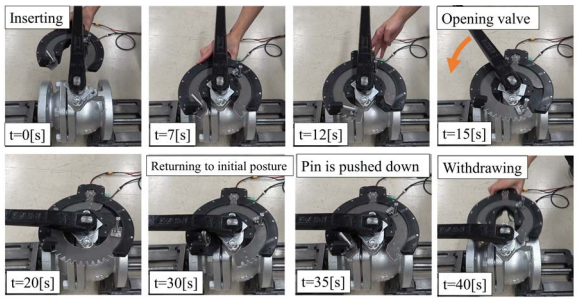

(a) Opening 80A ball valve.

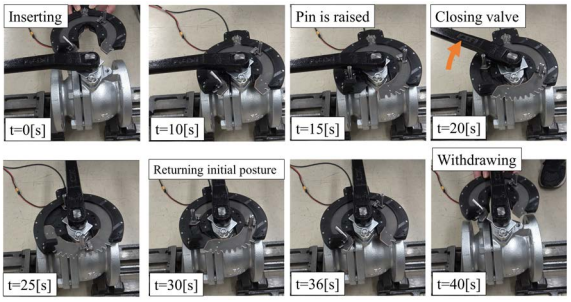

(b) Closing 80A ball valve.

Figure 26. Rotating a 80A ball valve with developed C-hand

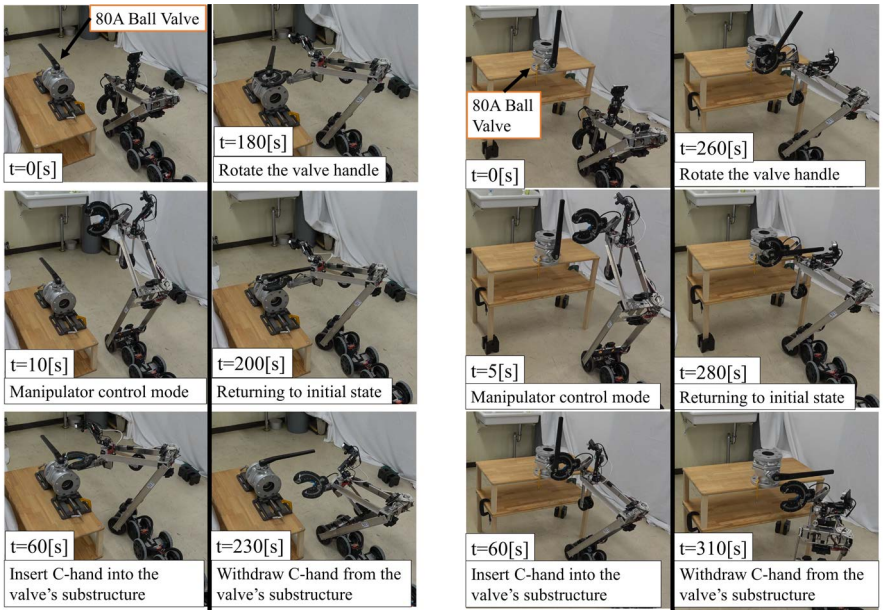

(a) Closing horizontal 80A ball valve.

(b) Closing vertical 80A ball valve.

Figure 27. Rotating 80A ball valve located at different height and orientation and position.

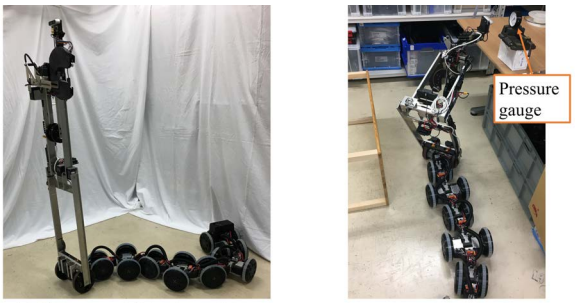

(a) The posture of the arm at its maximum height

(b) Reading pressure gauge from side

Figure 28. The posture of the folding arm during inspection.

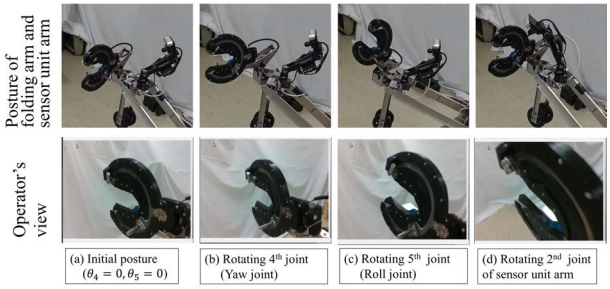

Figure 29. The posture of sensor unit arm according to the position of C-hand.

is also carried out. Figure 29 shows that the sensor unit could move based on the movement of C-hand, hence, the operator can always have a view on C-hand during the manipulator mode. In addition, Figure 29(d) also shows that the operator can move the sensor unit nearer to the C-hand to have a better view of it by rotating the second joint of the sensor unit arm.

4.5. Field test in WRS2020

We carried out experiments not only in the laboratory but also in the field test of the Plant Disaster Prevention Challenge in the World Robot Summit 2020 (WRS2020)[28]. The missions of the challenge are mainly the routine inspections in a mock industrial plant and initial response to emergency situations.

Figure 30 shows the proposed robot, T^2 Snake-4.2 performed plant inspection by reading the pressure gauges, checking the control panel LEDs of the pumps, inspecting rusted bolt on the flange of the pipes and finding abnormalities around pipes. The robot can read the pressure gauges and output a digital value of the pressure gauge by using image processing. However, the robot faced difficulty to read the pressure gauges automatically by using image processing because the folding arm with low rigidity was swinging due to the windy condition around the field.

The 80A ball valve in the mock industrial plant of WRS2020 was rusted and it needs alot more torque to rotate the valve handle. Figure 31 shows the proposed end effector, C-hand, was able to rotate the valve even in that condition. However, the robot fitted with C-hand could not rotate the valve during the competition. The operator could not insert C-hand into the valve's substructure because part of C-hand was stuck under

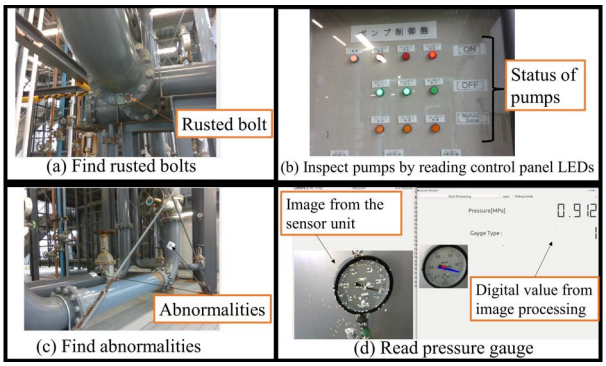

Figure 30. Images of the inspection and fault detection tests in WRS2020.

Figure 31. Operating 80A ball valve in WRS2020. (a) Rotating 80A ball valve by using C-hand. (b) Inserting C-hand into 80A ball valve's substructure with M2 arm

the valve handle. An additional experiment was conducted to understand the problem. Figure 32 shows the aerial view of proper insertion and bad insertion of C-hand into the valve's substructure. From the operator's view of the sensor unit, the operator could not see the part that was stuck under the valve handle.

The robot did not have sufficient time to climb stairs in the mock industrial plant because the proposed stairs climbing method is very time consuming. The improvement of the stairs climbing method of articulated mobile robot with folding arm is a task for future work.

5. Conclusion

We developed an articulated mobile robot T^2 Snake-4.2 for plant inspection. It is equipped with a novel folding arm, M2 arm, which improves the mobility of the robot compare to the previous version, T^2 Snake-4. By using proposed controller mode, the robot could climb up and down the step and stairs by contacting with the surrounding. In addition, the robot could reach high locations and perform inspection task with the sensor unit arm equipped on the folding arm.

We also developed a novel end effector C-hand to operate a large valve such as 80A ball valve in an industrial plant. C-hand is able to rotate the valve handle without transferring the reaction force to the robot.

The effectiveness of the developed arm was demonstrated by experiments and also tested in WRS2020. The robot was able to maneuver through narrow spaces in a mock plant. With the proposed system, the robot was able to carry out inspection tasks such

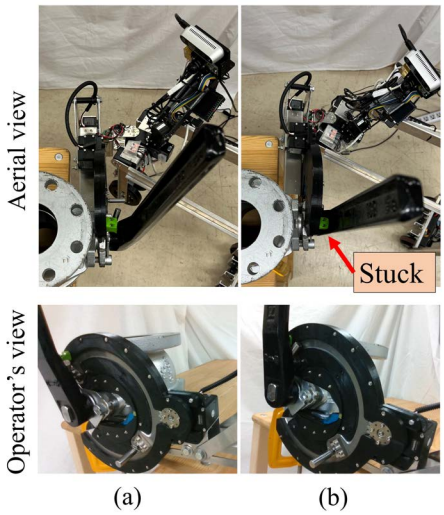

Figure 32. Comparison of proper insertion and bad insertion of C-hand. (a) Example of a proper insertion. (b) Example of a bad insertion.

as reading the value of the pressure gauges and inspect rusted bolts on a pipe flange. However, it is too time consuming for the robot to insert the C-hand into the valve's substructure and climbing stairs.

As a future task, we plan to improve the ability of the robot on adapting to a plant breakdown and a harsh environment such as rain and strong wind. We will consider replacing the actuators with waterproof and higher torque motors for better endurance. We also plan to improve the method of climbing stairs with the articulated mobile robot with a folding arm. In addition, C-hand proposed in this study can only operate the 80A Ball valve. We plan to review the design of C-hand and improve it to operate various types of valves in the future too.

Acknowledgement(s)

We like to thank all the team members of UEC-snake in WRS2020 for helping out with the maintenance and handling the robot during experiments and field tests.

References

[1] Kydd K, Macrez S, Pascal P. Autonomous Robot for Gas and Oil Sites. SPE Offshore Europe Conference and Exhibition; 2015 Sep 8-15; Aberdeen, Scotland, UK.

[2] Tadokoro S, Kimura T, Okugawa M, Oogane K, Igarashi H, Ohtsubo Y, Sato N, Shimizu M, Suzuki S, Takahashi T, Nakaoka S, Murata M, Takahashi M, Morita Y, Rooney EM. The World robot summit disaster robotics category –achievements of the 2018 preliminary competition. Advanced Robotics. 2019; 33(17): 854-875,

[3] Hutter M, Gehring C, Jud D, Lauber A, Bellicoso CD, Tsounis V, Hwangbo J, Bodie K, Fankhauser P, Bloesch M, Diethelm R, Bachmann S, Melzer A, Hoepflinger M. ANYmal - a highly mobile and dynamic quadrupedal robot. IEEE/RSJ International Conference on Intelligent Robots and Systems (IROS 2016); 2016 Oct 9-14; Daejeon, Korea; p. 38-44

[4] Hutter M, Diethelm R, Bachmann S, Fankhauser P, Gehring C, Tsounis V, Lauber A,

Guenther F, Bjelonic M, Isler L, Kolvenbach H, Meyer K, Hoepflinger M. Towards a Generic Solution for Inspection of Industrial Sites. In Field and Service Robotics. 2018; 575–589.

[5] Nagatani K, Kiribayashi S, Okada Y, Tadokoro S, Nishimura T, Yoshida T, Koyanagi E, Hada Y. Redesign of rescue mobile robot Quince. IEEE International Symposium on Safety, Security, and Rescue Robotics; Kyoto,Japan; 2011; p.13-18.

[6] Takemori T, Miyake M, Hirai T, Wang X, Fukao Y, Adachi M, Yamaguchi K, Tanishige S, Nomura Y, Matsuno F, Fujimoto T. Development of the multifunctional rescue robot FUHGA2 and evaluation at the world robot summit 2018. Advanced Robotics. 2020; 34(2): 119-131.

[7] Granosik G. Hypermobile Robots–the Survey. Journal of Intelligent & Robotic Systems. 2014; 75: 147–169.

[8] Osuka K, Kitajima H. Development of mobile inspection robot for rescue activities: MOIRA. IEEE/RSJ International Conference on Intelligent Robots and Systems (IROS 2003); Las Vegas, Nevada, USA; 2003; p. 3373-3377.

[9] Kamegawa T, Yamasaki T, Igarashi H, Matsuno F. Development of the Snake-like Rescue Robot 'KOHGA'. IEEE International Conference on Robotics and Automation; New Orleans, LA, USA; 2004; p. 5081-5086.

[10] Borenstein J, Hansen M, Borrell A. The OmniTread OT-4 Serpentine Robot – Design and Performance. Journal of Field Robotics. 2007; 24(7): 601-621.

[11] Arai M, Tanaka Y, Hirose S, Kuwahara H, Tsukui S. Development of "Souryu-IV" and "Souryu-V:" Serially connected crawler vehicles for in-rubble searching operations. Journal of Field Robotics. 2008; 25(1): 31-65.

[12] Suzuki K, Nakano A, Endo G, Hirose S. Development of Multi-wheeled Snake-like Rescue Robots with Active Elastic Trunk. IEEE/RSJ International Conference on Intelligent Robots and Systems; Algarve, Portugal; 2012; 4602-4607.

[13] Ito K, Maruyama H. Semi-autonomous serially connected multi-crawler robot for search and rescue. Advanced Robotics. 2016; 30(7): 489-503.

[14] Matsuno F, Kamegawa T, Qi W, Takemori T, Tanaka M, Nakajima M, Tadakuma K, Fujita M, Suzuki Y, Itoyama K, Okuno HG, Bando Y, Fujiwara T, Tadokoro S. Development of Tough Snake Robot Systems. In Springer Tracts in Advanced Robotics. 2019; 128: 267-326.

[15] Tanaka M, Nakajima M, Suzuki Y, and Tanaka K. Development and Control of Articulated Mobile Robot for Climbing Steep Stairs. IEEE/ASME Transactions on Mechatronics. 2018; 23(2): 531-541.

[16] Tanaka M, Tadakuma K, NakajimaM, Fujita M. Task-Space Control of Articulated Mobile Robots With a Soft Gripper for Operations. IEEE Transactions on Robotics. 2018; 35(1): 135-146.

[17] Yamada H, Hirose S. Development of Practical 3-Dimensional Active Cord Mechanism ACM-R4. Journal of Robotics and Mechatronics. 2006; 18(3): 305-311.

[18] Yamada H, Takaoka S, Hirose S. A snake-like robot for real-world inspection applications (the design and control of a practical active cord mechanism). Advanced Robotics. 2013; 27(1): 47-60.

[19] Kouno K, Yamada H, Hirose S. Development of Active-Joint Active-Wheel High Traversability Snake-Like Robot ACM-R4.2. Journal of Robotics and Mechatronics. 2013; 25(3): 559-566.

[20] Chiu Y, Shiroma N, Igarashi H, Sato N, Inami M, Matsuno F. FUMA: Environment Information Gathering Wheeled Rescue Robot with One-DOF Arm. IEEE International Safety, Security and Rescue Rototics. Kobe, Japan; 2005; p.81-86.

[21] Ueda K, Guarnieri M, Hodoshima R, Fukushima EF, Hirose S. Improvement of the remote operability for the arm-equipped tracked vehicle HELIOS IX. IEEE/RSJ International Conference on Intelligent Robots and Systems; Taipei, Taiwan; 2010; p.363-369.

[22] Kamezaki M, Ishii H, Ishida T, Seki M, Ichiryu K, Kobayashi Y, Hashimoto K, Sugano S, Takanishi A, Fujie MG, Hashimoto S, Yamakawa H. Design of Four-Arm Four-Crawler

Disaster Response Robot OCTOPUS. IEEE International Conference on Robotics and Automation (ICRA); Stockholm, Sweden; 2016; p.2840-2845.
[23] Fukushima EF, Hirose S, Hayashi T. Basic Manipulation Consideration For The Articulated Body Mobile Robot. IEEE/RSJ International Conference on Intelligent Robots and Systems; Victoria, Canada; 1998; p.386-393.
[24] Fukushima EF, Hirose S. Integration of Locomotion and Manipulation Control for Articulated Body Mobile Robots. Journal of Robotics Society of Japan. 2000; 18(8):1112-1121. Japanese.
[25] Tanaka M, Kon K, Nakajima M, Matsumoto N, Fukumura S, Fukui K, Sawabe H, Fujita M, Tadakuma K. Development and Field Test of the Articulated Mobile Robot T^2 Snake-4 for Plant Disaster Prevention. Advanced Robotics. 2020; 34(2):70-88.
[26] Matsumoto N, Tanaka M, Nakajima M, Fujita M, Tadakuma K. Development of a folding arm on an articulated mobile robot for plant prevention. Advanced Robotics. 2020;34(2):89-103.
[27] Fujita M, Tadakuma K, Komatsu H, Takane E, Nomura A, Ichimura T, Konyo M, Tadokoro S. Jamming Layered Membrane Gripper Mechanism for Grasping Differently Shaped-Objects Without Excessive Pushing Force for Search and Rescue. Advanced Robotics. 2018; 32(11):590-604.
[28] WRS2020 FUKUSHIMA, World Robot Challenge[Internet].Japan; [cited 2022 Jan 13]. Available from: `https://wrs.nedo.go.jp/fukushima/`
[29] Takahashi T, OkadaY, Kojima S, Tadakuma K, Watanabe M, Takahashi M, Tadokoro S. Design and Control of Parallel Gripper with Linear and Curved Trajectory Consisting of Only Revolute Pairs. IEEE/SICE International Symposium on System Integration (SII); Honolulu, Hawaii, USA; 2020; p.557-562.
[30] Yamada H, Hirose S. Study of Active Cord Mechanism -Approximations to Continuous Curves of a Multi-joint Body-. Journal of the Robotics Society of Japan. 2008; 26(1):110-120. Japanese.
[31] Kucuk S, and Zafer B. Robot kinematics: Forward and inverse kinematics. Industrial Robotics: Theory, Modelling and Control. InTech. 2006;117-148.
[32] Waldron K. Schmiedeler J. Kinematics. In: Siciliano B., Khatib O. (eds) Springer Handbook of Robotics. Springer, Berlin, Heidelberg; 2008; p.11-35.
[33] Plant Disaster Prevention Challenge DAY1 (October 8, 2021)[Internet]. World Robot Summit; [cited 2022 Jan 13]. Available from:`https://youtu.be/BVsZyMuyGFE?t=11461`
[34] Plant Disaster Prevention Challenge DAY2 (October 9, 2021)[Internet]. World Robot Summit; [cited 2022 Jan 13]. Available from: `https://youtu.be/-iL8MLIVCOY?t=12698`